

8. HYDROSTATIC CONSOLIDATION TESTS OF UNDEFORMED, CLAY-RICH SAMPLES FROM THE BARBADOS ACCRETIONARY PRISM, LEG 156¹

Peter Vrolijk,² Terry Miller,² and M.J. Gooch²

ABSTRACT

Geomechanical tests of three well-characterized, clay-rich, macroscopically undeformed samples document the loading history and permeability of two late Miocene samples above the décollement zone and a late Oligocene sample below the décollement zone of the Barbados accretionary prism. These samples are similar in all aspects studied. About two-thirds of each sample is clay, of which most is mixed-layer illite/smectite. Permeabilities are low, ranging from 5×10^{-18} to 1×10^{-19} m². All samples are underconsolidated and may have been overpressured since shortly after deposition, especially the late Miocene sample near the deformation front (Site 949). Alternatively, the apparent low consolidation state may arise from disruption of grain contacts by early deformation in the accretionary prism, thereby erasing any earlier stress history.

INTRODUCTION

There is an intimate link between a sediment's mineralogic composition, its response to stress and stress history, and its hydrologic and transport properties. We seek to elucidate these relations further through geomechanical testing of macroscopically undeformed, well-characterized, clay-rich rocks from the Barbados accretionary prism. Our samples come from two holes and include shallow and deep samples taken both above and below the décollement zone (Tables 1–3). The shallow sample above the décollement zone comes from Hole 949C, drilled 2 km west of the deformation front. The other samples are from Hole 948C, which was drilled next to Site 671 (Ocean Drilling Program [ODP] Leg 110) 4 km arcward of the leading edge of deformation.

Experimental Strategy

The experimental program was designed to determine the samples' vertical permeability at various effective stress levels, their previous maximum effective stress level, and their undrained shear strength. Data were collected throughout the undrained shear tests so that the stress path to failure could be constructed and compared with predictions from Critical State Soil Mechanics Models (Atkinson and Bransby, 1978).

Permeability was determined from the samples' consolidation response; in one case (156-948C-13X-3, 60–70 cm), permeability was also determined by a constant-head test. The permeability measurement derived from consolidation is based on a modification of Terzaghi's solution to the one-dimensional consolidation equation. In this solution, the sample's permeability is determined from the volume and stress changes during a given stress increase and from the time required for the sample's volume to change at each load step. The solution is modified to account for the fact that stresses are changed isotropically while flow is still one dimensional. The modification is simple in that the volume changes are computed based on the sample's isotropic compressibility, rather than the constrained, uniaxial compressibility used in Terzaghi's derivation. The permeability is given by

$$k = \frac{\Delta v \cdot l^2}{v \cdot \Delta \sigma_m \cdot \mu \cdot t_{100}},$$

where v is the sample volume, l is the drainage length (which equals one-half the sample length in this case with double drainage), σ_m is the mean effective stress ($(\sigma_v + 2\sigma_h)/3$), μ is the pore-fluid viscosity, and t_{100} is the time required for the sample to attain 100% consolidation for the applied stress.

This method typically produces repeatable measurements, but it can introduce errors over certain stress ranges because it assumes that permeability and compressibility are constant over a given load step. These assumptions are typically less valid at low effective stress levels and at load stages in which plastic yielding takes place. The error magnitude depends on the sample's behavior, but the error typically becomes smaller as the sample loading increases. In a later section we conclude that permeabilities inferred at the higher tested stress levels most closely approximate in situ permeabilities. Others (e.g., Moran et al. [1995] and Fisher et al. [1994]) have noted that permeabilities measured in constant flow-rate tests conducted at low flow rates can differ by as much as 2 orders of magnitude from the permeabilities calculated from the consolidation response. These large differences typically occur at lower effective stresses, however, and the values obtained by the two measurement techniques tend to converge at higher stress levels.

METHODOLOGY

Mineralogy

We took ~3-g samples next to the test cylinders for mineralogical analysis. For each sample, we measured an X-ray-diffraction (XRD) pattern on the bulk sample and a <0.2-mm-sized separate (Table 1); all diffraction peaks on the bulk XRD pattern were assigned to a mineral. Clay (<0.2 mm) fractions were analyzed in air-dried and glycolated states after heating to 50°C for 5 hr. A split of the whole-rock sample was analyzed for all major and some minor elements by X-ray fluorescence (XRF; Tables 2, 3). In addition, a split of each sample was analyzed by He-pycnometry to determine grain densities, and another split was used to measure weight loss during heating by thermogravimetric analysis (TGA).

XRD mineral occurrence data were combined with XRF elemental abundance data to calculate quantitative mineral abundances. This

¹Moore, J.C., Klaus, A., et al., 1998. *Proc. ODP, Init. Repts.*, 171A: College Station, TX (Ocean Drilling Program).

²Exxon Production Research Company, P.O. Box 2189, Houston, TX 77252-2189, U.S.A. peter.j.vrolijk@exxon.sprint.com

procedure works best for rocks that contain minerals with well-defined chemical stoichiometries. For example, sandstones that contain quartz, K-feldspar, calcite, some clay cements, and so forth, can be analyzed with relative errors of 3% for minerals >50%, 10% for minerals 10%–50%, and 3% for minerals <10% (absolute error) of the sandstone sample. Clay-rich rocks contain minerals with variable composition; thus, no single solution of the combined XRD and XRF data is unique.

Clay mineral abundances were further evaluated by calculating XRD patterns for clay-mineral mixtures, using the XRD algorithms of Reynolds (1985) and comparing those patterns with measured patterns. Reported values of percent illite (%I) in illite/smectite (I/S) were derived from this modeling effort.

The amount of smectite in each sample was further evaluated by TGA. In this analysis, the sample is exposed to hydrated air flowing over the sample at 20 mL/min for 60 min before the analysis begins. The sample is then heated at a rate of 5°C/min to 964°C, and the weight is monitored. These data were used to qualitatively confirm interpretations derived from the procedures described above.

Mechanical Testing

Test samples were prepared from the ~15-cm-long, whole-round core as follows. The cores were sawed into two 7.5-cm pieces, and three lubricated, 2.5-cm diameter, thin-walled sample tubes were pressed through the core pieces. Before testing, the sample tubes were removed from the core pieces, and the samples were gently extruded from the tubes. Unneeded core pieces were then returned to a 100% relative humidity chamber for storage. The extruded samples were trimmed to a nominal 5-cm length with parallel ends and weighed, and their exact dimensions were measured.

The samples were then placed between load platens and jacketed with a polyolefin, heat-shrink tubing. Clip-on radial and axial displacement gauges were then mounted on the tubing, and the whole assembly was placed in the triaxial-test vessel. The pore-pressure system was placed on vacuum while the triaxial-test vessel was filled with oil. After filling the vessel, the confining pressure was increased to 70 kPa while saline pore fluid was circulated through porous stones on each load platen. After the pore-pressure system was saturated, the pore and confining pressures were increased simultaneously by 350 kPa to pressure-saturate the samples.

Saturation was assumed to be complete when a B-coefficient (Bishop and Henkel, 1974) greater than 0.98 was attained. Hydrostatic consolidation steps of various mean-stress increments were then applied to the sample. We chose to test the samples under hydrostatic stress conditions (axial and radial stresses equal) rather than K_0 stress conditions (no radial strain), a stress state often assumed in the Earth for porous materials (Atkinson and Bransby, 1978), because hydrostatic loading allowed us to evaluate permeability at a constant stress value. K_0 stress loading would have produced continuously changing stress conditions that would have made estimates of permeability impossible.

The pressure transducers used in these tests were designed for normal operation at pressures in excess of 7000 kPa; thus, we were unable to maintain an accuracy of $\pm 10\%$ of mean-stress increments at stresses less than 140 kPa. After samples had been consolidated to their desired mean-stress level, the pore-fluid system was isolated, and axial stress was increased until the sample was effectively unable to carry more load. Sample axial strain rates of $10^{-6}/s$ were slower than the recommended rates given by Bishop and Henkel (1974), as determined from the consolidation response.

During the undrained testing, pore pressure was measured by a small-displacement pressure transducer mounted outside the triaxial-test vessel. Excess volume in the pore-fluid system was minimized to about 10% of the sample's pore volume by the use of capillary tubing to connect the pressure transducer to the sample's ends.

Most permeability data presented here are derived from the consolidation response of samples during load increments (see above). Permeability was measured in a constant-head test on one sample (156-948C-13X-3, 60–70 cm). In this test, permeability was measured by first subjecting a 1.4-cm-long sample to a nominal confining pressure of 689 kPa with a back pressure of 69 kPa, and then allowing it to consolidate at that stress level. Fluid was then pumped into one end of the sample at a constant flow rate of 0.001 cm³/min until the flow out of the sample reached a steady-state at the same rate. Sample permeability was then determined based on the flow rate and pressure drop across the sample. In this case, the flow rate was selected so that the resulting increased pore pressure at the upstream end of the sample did not exceed the nominal confining pressure. Because of time constraints, the test included only one flow rate. We expect that other flow rates would have resulted in different effective stresses across the sample and would have caused a different permeability structure in the sample.

RESULTS

Mineralogy

The three tested samples are clay rich, with clay minerals composing 63%–71% of the sample (Table 1). Illite/smectite (a Reichweite = 0 mixed-layer I/S) is the main clay and bulk mineral and makes up about one-third of each sample (Table 1); I/S consists of 45%–82% smectite (Tables 1–3). Discrete, detrital illite and kaolinite are the next most important mineral types. Quartz, plagioclase, calcite, and hematite are the remaining important mineral constituents. TGA data indicate that hydrated amorphous materials constitute an important fraction of these samples because 4.7%–6.1% of the samples' weights are lost by the time they reach 100°C. By comparison, pure montmorillonite (SWy-1) loses 6.7% of its weight over the same temperature range. However, XRD data indicate that the samples are <50% smectite, rather than near 90%.

Test Results

Samples from each core interval were subjected to two to nine load increments. At the end of each load stage, the final mean effective stress was recorded and the void ratio and permeability were calculated. Test results are presented in Table 4. Note that we present results for three different subsamples of Sample 156-948C-13X-3, 60–70 cm, (Subsamples a, b, and c).

Maximum Previous Mean Effective (Preconsolidation) Stress

In many cases, two linear segments contribute to a plot of a sediment's void ratio vs. the logarithm of the mean effective stress, as measured in a series of isotropic consolidation (hydrostatic stress-state) tests. The intersection of these segments is interpreted as the value of the maximum effective stress experienced by that sediment before testing (Atkinson and Bransby, 1978). This maximum value is termed the preconsolidation stress, σ_{mpc} . The existence and sometimes the timing of overpressures can be inferred from the preconsolidation stress and the value of the mean effective stress for a normally consolidated material (σ_{mnp}) at the sediment's current burial depth. When σ_{mnp} is greater than σ_{mpc} , it is usually assumed that excess pore pressures are caused by rapid burial and restricted fluid flows.

Figures 1 through 3 include plots of the void ratio vs. the log of the mean effective stress for Samples 156-948C-3X-3, 89–102 cm; 156-949B-3X-2, 87–101 cm; and 156-948C-13X-3, 60–70 cm, respectively. The plots for Samples 156-948C-3X-3, 89–102 cm, and 156-949B-3X-2, 87–101 cm, from depths of 434 and 266 mbsf, respectively—as well as above the décollement zone—indicate that Sample 156-948C-3X-3, 89–102 cm, has a preconsolidation stress of

Table 1. Mineralogical analyses of sediments used in geomechanical tests.

Core, section, interval (cm)	Sample depth (mbsf)	Age	Structural position	Clays										
				Quartz	Plagioclase	Calcite	Hematite	Kaolinite	Illite	Smec	%I(I/S)	Illite (detrital)	I/S	Total clay
156-948C-3X-3, 89-102	434.39	late Miocene	A	12	6	1	6	7	29	35	18	24	40	70
13X-3, 60-70	530.40	late Oligocene	B	12	3	15	4	15	29	19	55	13	35	63
156-949B-3X-2, 87-101	265.87	late Miocene	A	12	5	0	6	14	30	24	35	20	34	68

Table 1 (continued).

Core, section, interval (cm)	Sample depth (mbsf)	Age	Porosity Total (%)	Grain density (kg/m ³)	
					156-948C-3X-3, 89-102
13X-3, 60-70	530.40	late Oligocene	97	56	2703
156-949B-3X-2, 87-101	265.87	late Miocene	91	64	2713

Notes: Bulk mineralogy determined from optimizing mineral abundances based on bulk XRD patterns, bulk sample chemistry, and assumed mineral stoichiometry. I = illite; S = smectite. Clay mineral abundances determined from modeling bulk sample chemistry and <0.2- μ m XRD pattern, consideration of sample surface area, and qualitative analysis of TGA. Illite and smectite percentages in italics are idealized end-member results. Information on %I(I/S) from a modeled <0.2- μ m XRD pattern used to calculate amount of detrital illite and mixed-layer I/S. Structural position: A = above the décollement zone; B = below the décollement zone. Pycnometry analyses were performed after samples were dried at 100°C, disaggregated by light grinding, further dried in cell holder at 95°C, and then cooled in a desiccator. We obtained a density of 2645 kg/m³ for a quartz standard.

Table 2. Major element chemical analyses of sediments used in geomechanical tests.

Core, section, interval (cm)	Sample depth (mbsf)	Age	Structural position	C (%)	C _{org} (%)	Na ₂ O (%)	MgO (%)	Al ₂ O ₃ (%)	SiO ₂ (%)	P ₂ O ₅ (%)	S (%)	K ₂ O (%)	CaO (%)	TiO ₂ (%)
156-948C-3X-3, 89-102	434.39	late Miocene	A	0.14	0.08	0.53	3.00	18.4	53.3	0.09	0.05	2.39	0.88	0.812
13X-3, 60-70	530.40	late Oligocene	B	2.04	0.40	0.32	1.52	17.8	46.7	0.13	0.26	2.19	8.86	0.669
156-949B-3X-2, 87-101	265.87	late Miocene	A	0.14	0.11	0.36	2.45	19.4	49.7	0.14	0.04	2.25	0.74	0.760

Table 2 (continued).

Core, section, interval (cm)	Sample depth (mbsf)	Age	Cr ₂ O ₃ (%)	MnO (%)	Fe ₂ O ₃ (%)	LOI (%)	Sum (%)
156-948C-3X-3, 89-102	434.39	late Miocene	<0.01	0.08	8.19	12.7	100.4
13X-3, 60-70	530.40	late Oligocene	<0.01	0.08	6.27	15.7	100.4
156-949B-3X-2, 87-101	265.87	late Miocene	0.02	0.13	8.70	15.7	100.4

Note: Structural position: A = above the décollement zone; B = below the décollement zone.

Table 3. Minor element chemical analyses of sediments used in geomechanical tests.

Core, section, interval (cm)	Sample depth (mbsf)	Age	Structural position	Rb (ppm)	Sr (ppm)	Y (ppm)	Zr (ppm)	Nb (ppm)	Ba (ppm)
156-948C-3X-3, 89-102	434.39	late Miocene	A	99	100	28	118	<10	287
13X-3, 60-70	530.40	late Oligocene	B	119	402	34	117	17	510
156-949B-3X-2, 87-101	265.87	late Miocene	A	98	103	31	133	12	271

Note: Structural position: A = above the décollement zone; B = below the décollement zone.

nominally 207 kPa, whereas Sample 156-949B-3X-2, 87–101 cm, has a preconsolidation stress less than 69 kPa. These preconsolidation stresses compare with calculated values of σ_{mnp} of at least 2029 and 1242 kPa, respectively, for sediments at these same burial depths (Table 5). These values are calculated assuming a “lithostatic” stress curve for Site 948 (Moore et al., 1995), a pore-water specific gravity of 1.04, equal horizontal stresses, and horizontal effective stresses are

65% of vertical effective stresses. This assumed value of the ratio of horizontal to vertical effective stress during compaction is consistent with measured values for many clay-dominated sediments (Scofield and Wroth, 1968) and should be a lower bound to the σ_{mnp} found in a thrust zone and to the σ_{mnp} measured in a hydrostatic consolidation test (Atkinson and Bransby, 1978). Moreover, calculated σ_{mnp} values of late Miocene sediments at Site 672, which are undeformed, range

Table 4. Test results of “undeformed” mudstone samples.

Core, section, interval (cm)	Depth (mbsf)	Age	Structural position	Core plug	Load stage	Final mean effective stress (kPa)	Void ratio	Permeability (m ²)
156-948C-3X-3, 89-102	434.39	late Miocene	A	a	0	69	1.41	
					1	207	1.40	1.54 ⁻¹⁸
					2	724	1.26	5.15 ⁻¹⁸
					3	2000	1.12	9.54 ⁻¹⁹
13X-3, 60-70 (Subsample a)	530.40	late Oligocene	B	a	0	241*		
					0	88	1.28	4.90 ⁻¹⁹
				b	1	241	1.26	2.71 ⁻¹⁹
					2	505	1.16	2.74 ⁻¹⁹
13X-3, 60-70 (Subsample c)	530.40	late Oligocene	B	c	0	46	1.14	
					1	267	1.04	2.96 ⁻¹⁸
					2	452	1.01	4.22 ⁻¹⁹
					3	817	0.96	5.77 ⁻¹⁹
					4	1161	0.92	3.66 ⁻¹⁹
					5	2072	0.86	3.41 ⁻¹⁹
					6	3818	0.77	1.96 ⁻¹⁹
					7	6890	0.64	1.35 ⁻¹⁹
156-949B-3X-2, 87-101	265.87	late Miocene	A	a	0	69	1.78	
					1	103	1.70	5.00 ⁻¹⁸
					2	248	1.58	1.98 ⁻¹⁸
					3	455	1.48	7.05 ⁻¹⁹
					4	34	1.59	No data
					5	379	1.51	3.71 ⁻¹⁹
					6	690	1.44	2.65 ⁻¹⁹
					7	34	1.57	No data
					8	690	1.44	4.15 ⁻¹⁹
9	876	1.39	4.26 ⁻¹⁹					

Notes: Structural position: A = above the décollement zone; B = below the décollement zone. Core plugs a, b, and c = vertical plugs subsampled from whole-round core. Load stage initial value = 0. * = average stress in constant-head test.

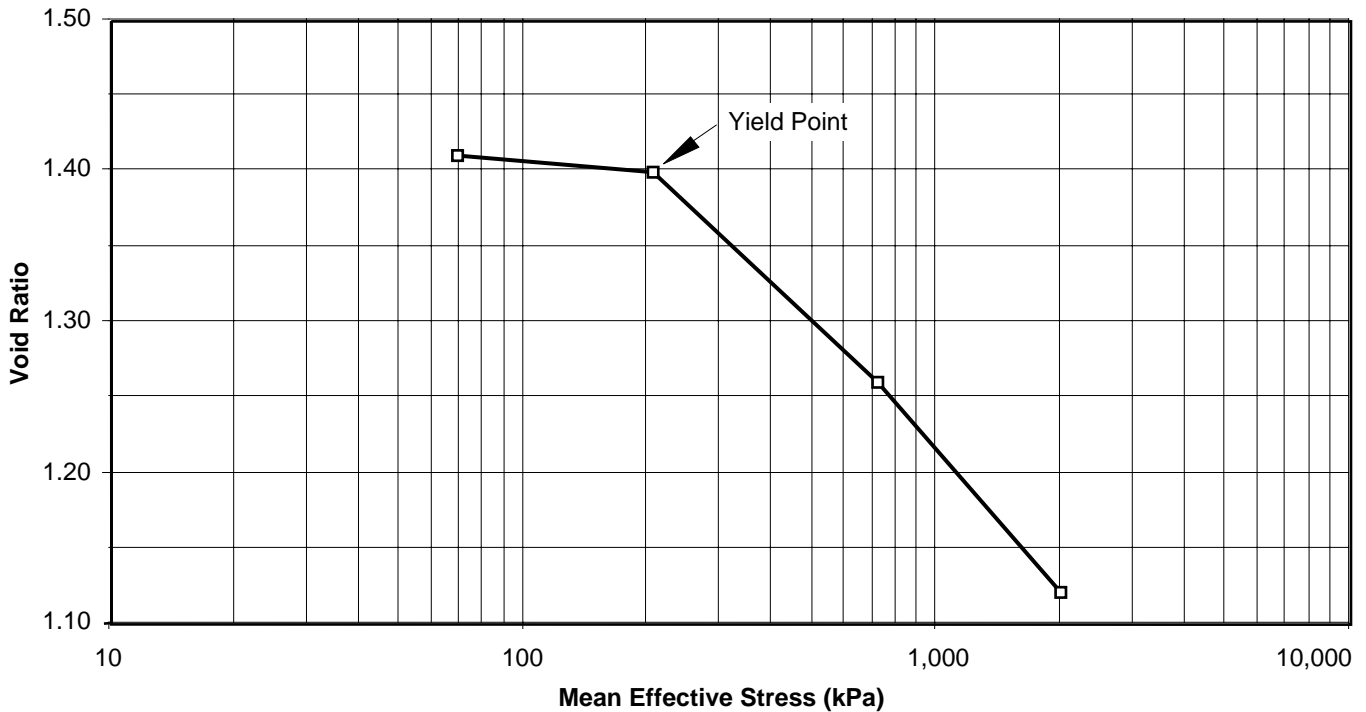


Figure 1. Void ratio vs. mean effective stress. Sample 156-948C-3X-3, 89–102 cm. Kink in line = value of preconsolidation stress σ_{mpc} at 207 kPa.

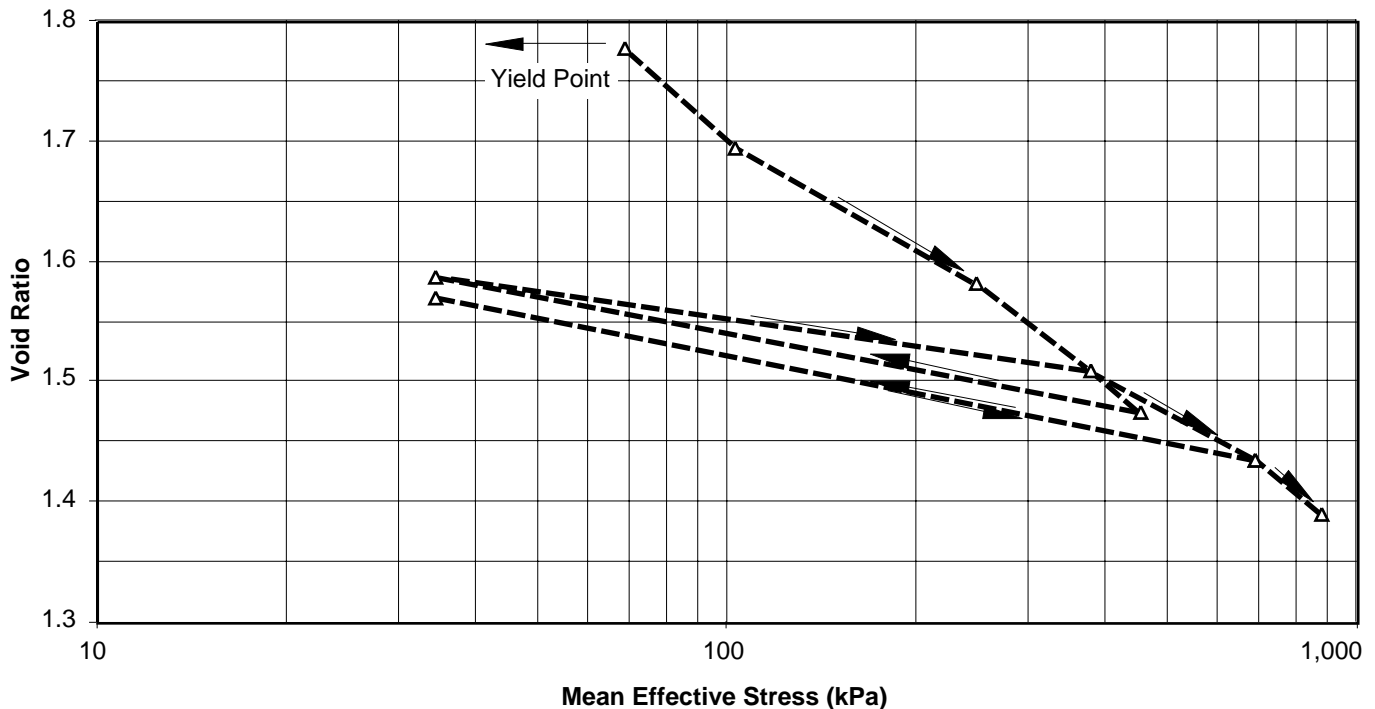


Figure 2. Void ratio vs. mean effective stress. Sample 156-949B-3X-2, 87–101 cm. Two points with void ratios between 1.55 and 1.6 and mean effective stress of 34 kPa represent interruptions in the test. Note how the line described by most data is straight; we interpret a preconsolidation stress <69 kPa for this sample.

from 481 to 646 kPa (Table 5); these values represent approximate stresses seen by the samples before deformation in the accretionary prism.

Figure 3 is the void ratio vs. log-mean effective stress for Sample 156-948C-13X-3, 60–70 cm, from a depth of 530 m, which falls below the décollement zone. This plot indicates that Sample 156-948C-13X-3, 60–70 cm, has a preconsolidation stress of 1993 kPa. The value of σ_{mmp} for this sample is 3300 kPa, whereas σ_{mmp} for late Oligocene samples at Site 672 is 1275 kPa (Table 5). The excess of σ_{mmp} over σ_{mpc} for this sample is proportionally greater than that seen in the samples retrieved above the décollement zone. This finding is consistent with a rapid burial rate for this sample, but does not require that overpressures develop before the onset of deformation.

Permeability

Figure 4 is a plot of the samples' permeabilities vs. their mean effective stresses. Permeability values are calculated from the samples' consolidation responses as discussed above, and the data points are plotted against the mean effective stress at the end of each consolidation step. The permeability marked by a single data point was determined by the constant-head, flow-through test on a companion piece to Sample 156-948C-13X-3, 60–70 cm; here the mean stress is the sample's average effective stress. Note that the permeabilities inferred from the constant-head test and the consolidation response differ only by a factor of 2 (Fig. 4). In samples where permeability drops by an order of magnitude as higher mean effective stresses are applied (e.g., Sample 156-949B-3X-2, 87–101 cm), we interpret in situ permeabilities that correspond to the in situ mean effective stresses.

In addition, something other than porosity appears to control permeability of these samples. Although Samples 156-948C-3X-3, 89–102 cm, and 156-949B-3X-2, 87–101 cm, have equivalent porosities of about 60%, their permeabilities differ by about an order of magnitude. Conversely, Samples 156-948C-13X-3, 60–70 cm, and 156-949B-3X-2, 87–101 cm, have essentially the same permeabilities, even though their porosities are ~50% and 60%, respectively. Al-

though all of these samples have relatively high smectite content (35%–40% I/S; Tables 1–3), Sample 156-948C-3X-3, 89–102 cm, has a higher smectite content, an intermediate porosity, and a higher permeability than the other samples.

Undrained Shear Strengths

Figure 5 is a plot of the stress paths for the undrained shear-strength tests on the three samples. Note that the stress paths for the consolidation phases of these tests is nominally along the mean effective stress axis. There is a nominal shear stress component to these paths because the axial stress was maintained at 20 to 30 kPa higher than the confining pressure to ensure that the loading platens were always in contact with the test specimens. The stress paths in Figure 5 are plotted in terms of the differential axial stress, q ($\sigma_a - \sigma_r$), vs. the mean effective stress, σ_m . We estimate that the shear strength of these samples is given by the data points located near the inflections in the stress-path plot where q and σ_m both increase at the same time.

The inflection points on the q vs. σ_m plot coincide with a work-hardening point on a stress-strain curve (Fig. 6) and with the point where pore pressure becomes constant. Constant pore pressure could indicate that the samples have reached critical state (i.e., constant volume deformation). The work-hardening aspect of the stress-strain curve is problematic; based on later tests in our laboratory, we suspect that in some cases the radial strain gauge may exert an additional confining pressure, causing constriction of the sample at the circumference of the strain gauge. This could create the sudden appearance of apparent work-hardening behavior in the stress-strain history and a positive slope for q vs. σ_m .

The solid line in Figure 5, which was constructed to connect the failure points of each sample tested, represents a critical-state line. The fact that it can model the critical-state points for all three of the samples suggests that there are no strong differences in the stress-strain response among these samples. The slope of the critical-state line, μ , is ~0.75, corresponding to an angle of internal friction of about 20°. The value of μ is consistent with that of high plasticity

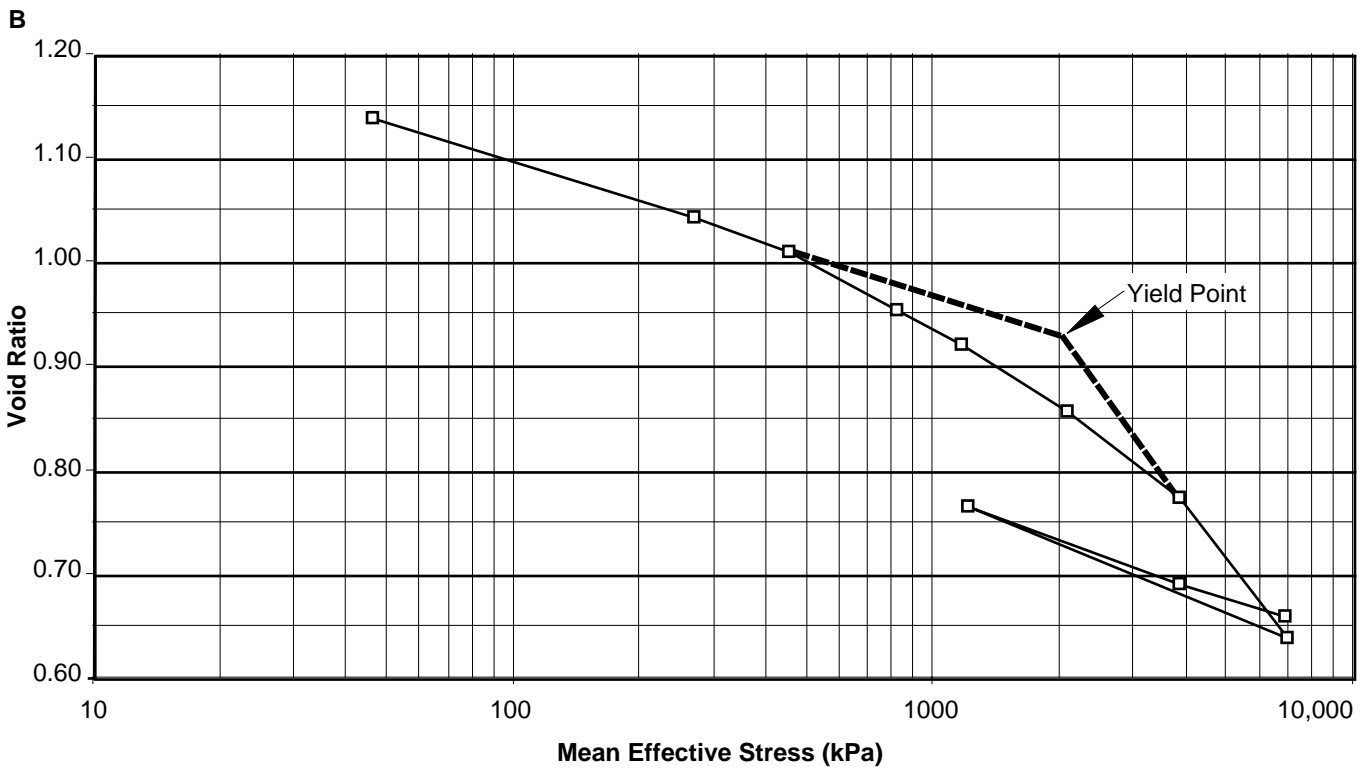
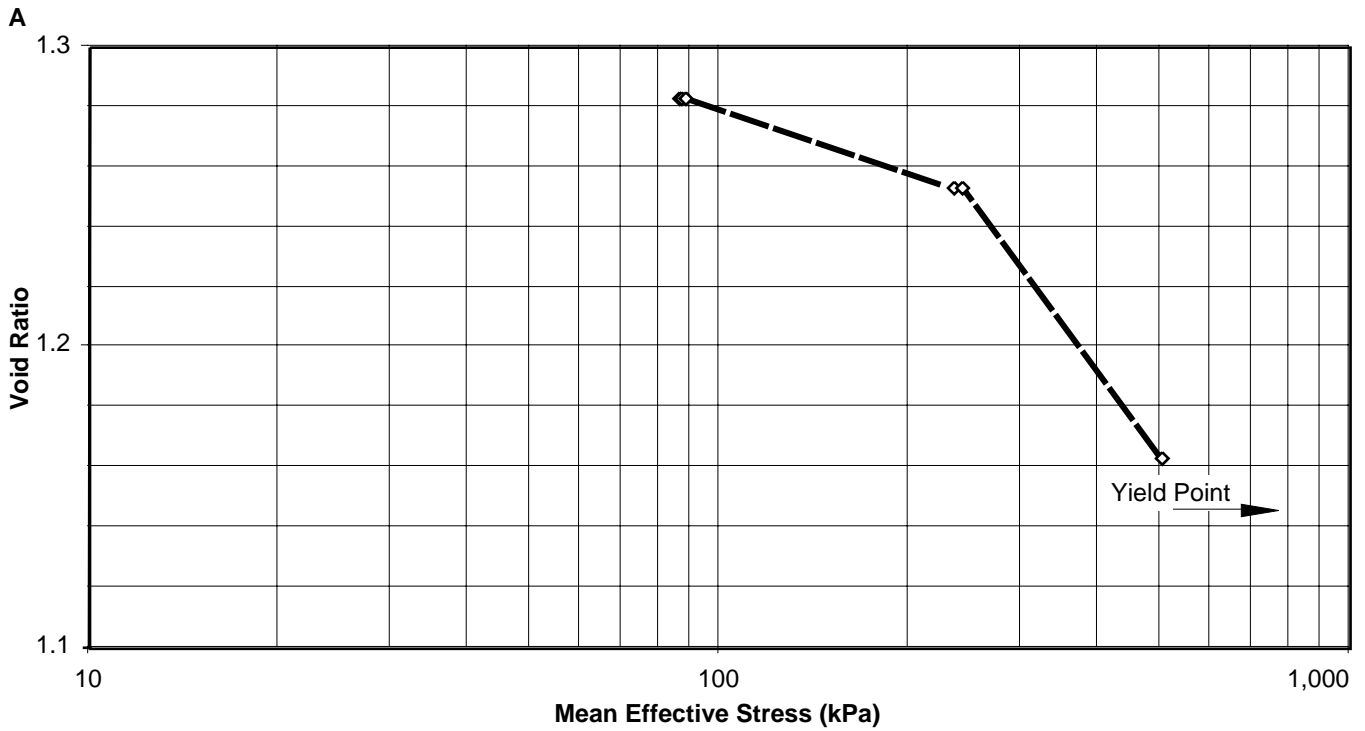


Figure 3. Void ratio vs. mean effective stress. Sample 156-948C-13X-3, 60–70 cm. **A.** Subsample a: Kink in line was initially interpreted as the yield point; subsequent tests proved this interpretation wrong. Shear strength test, recorded in Figure 4, was performed at the conclusion of this test. **B.** Subsample c: Preconsolidation stress was picked at 1993 kPa for this sample.

Table 5. Preconsolidation stresses of “undeformed” mudstone samples.

Core, section, interval (cm)	Depth (mbsf)	Measured σ_{mpc} (kPa)	Calculated σ_{mnp}	
			in situ	Site 672
156-948C- 3X-3, 89-102	434.39	207	2029	481-646
156-949B- 3X-2, 87-101	265.87	<69	1242	481-646
156-948C- 13X-3, 60-70	530.40	1993	3300	1275

Notes: Calculated values of σ_{mnp} at Site 672 are based on depth assignments of 115–143 mbsf for Miocene samples and 239 mbsf for the Oligocene sample. These values are presented to contrast stress values assumed before the imposition of thrust and thrust-loading stresses with those that follow.

clays (Scofield and Wroth, 1968), a fact which is also consistent with these samples' high smectite content.

Subsample a of 156-948C-13X-3, 60–70 cm, appears to be stronger than the others (relative to the inferred failure line). However, the shear strength test for this sample was one of the first performed. During the test, we mistakenly concluded that the sample was fully consolidated, and we initiated the shear test. Subsequent tests revealed that the sample had become only partially consolidated. Subsample c from that core sample was rerun to full consolidation; those results are presented in the consolidation section. Unfortunately, a power failure terminated the test before the sample could be tested in shear. Thus, the shear test presented in Figure 5 represents the shear strength of a somewhat overconsolidated sample.

DISCUSSION OF RESULTS

These three samples represent the oldest and deepest samples of the Barbados accretionary prism that have been tested to date. Our analyses indicate that these samples are similar in their mineralogy and petrophysical and deformation responses. In this discussion, we compare our results with previous analyses and speculate on the implications of these results.

Mineralogy

Our analyses differ from the shipboard analyses in the following ways:

1. We consistently find less quartz in these samples than was indicated by shipboard analyses (Shipley, Ogawa et al., 1995); differences range from 13% to 18%.
2. We find less smectite, relative to illite, in each of our analyses; smectite is 1.5–3 times more abundant than illite in our analyses, but 1.5–4 times more abundant in the shipboard analyses.

We think our results provide a more accurate representation of the mineralogy of these samples, because we have attempted to reconcile multiple analytical procedures in our mineralogical assessment, including XRD mineral identification, XRF elemental analysis, quantitative XRD analysis of oriented clay fractions, and thermogravimetric analysis. Shipboard analyses rely only on XRD patterns calibrated against artificial mixtures of relevant minerals (Fisher and Underwood, 1995). Moreover, we attempt to determine mineral abundances on a whole-sample basis; shipboard analyses are normalized to a limited set of calibration minerals. Notice, though, that the differences between the methods are small, especially considering that the foregoing comparisons are based on samples separated by tens of centimeters.

In spite of these efforts, the values in Tables 1 through 3 still contain some unspecified uncertainty. One indication of that uncertainty is our inability to achieve a 100% total mineral abundance, even

though XRF analyses recorded 100% of the samples. Part of this uncertainty arises from our inability to model amorphous phases that must be present in the rock, based on loss-on-ignition and TGA results. The nature and amount of amorphous materials have never been quantified in samples from the Barbados accretionary prism, but they appear to decrease in abundance with increasing sediment age.

Consolidation Response

Taylor and Leonard (1990) performed one-dimensional consolidation tests on a wide range of samples from ODP Leg 110. In most of their tests, they determined a preconsolidation stress of 100–500 kPa, results similar to those from our samples. However, Taylor and Leonard (1990) found preconsolidation stresses <100 kPa only in Pleistocene samples. Moran and Christian (1990) performed triaxial tests on Pliocene–Pleistocene samples from ODP Leg 110. They found similar preconsolidation stresses of 100–400 kPa and stresses <100 kPa for Pleistocene samples only. Thus our observation of negligible preconsolidation stress for Sample 156-949B-3X-2, 87–101 cm, is remarkable.

For our samples, the degree of overpressuring, as measured by the difference between σ_{mpc} and σ_{mnp} , appears to increase with increasing burial depth. One interpretation of this finding is that overpressuring commenced soon after deposition and has slowly increased as burial depth has increased. Note that because the measured preconsolidation stresses for the samples are less than those calculated for normally pressured samples at Site 672, pore pressures rose above hydrostatic before deformation began. This interpretation is consistent with the observed low values of sediment permeability measured on these samples. Alternatively, the apparent lack of a preconsolidation stress for Sample 156-949B-3X-2, 87–101 cm, could indicate recent high strain-rate deformation at the deformation toe. In this case, deformation has disrupted grain contacts and caused the material to lose any memory of earlier burial history. However, macroscopic observations of core specimens offer no evidence of deformation. Similar triaxial consolidation tests of samples from an undeformed reference site could help establish the degree of overpressure developed before deformation begins.

Moran and Christian (1990) determined a failure envelope for the samples they analyzed (Fig. 5). Their failure envelope has a slightly steeper slope than the critical-state line we determined; for normally and underconsolidated sediments, the failure envelope and critical-state line are the same. The difference between Moran and Christian's line and ours may result from the different sediment lithologies analyzed in each study. Moran and Christian restricted their analyses to Pliocene–Pleistocene samples that contain calcite fossils, whereas our Miocene samples are calcite free.

Permeability

We inferred permeabilities ranging from 5×10^{-18} to 1×10^{-19} m². Permeability determined from a single constant-head test compares well with that inferred from consolidation response (Table 4; Sample 156-948C-13X-3, 60–70 cm). Taylor and Leonard (1990) also determined permeabilities, but their results ranged from 10^{-14} to 10^{-20} m². Restricting their results to clay and mudstone samples with void ratios between 1 and 1.5 (the range we observed), two populations of results emerge: one with a permeability of 10^{-14} to 10^{-15} m², and one at 10^{-17} to 10^{-19} m². Our results are consistent with the lower permeability population. Our permeability measurements are also the same as those inferred by Sreaton et al. (1990) and Wuthrich et al. (1990), given the assumption of near-lithostatic fluid pressures at Site 542.

SUMMARY

Two samples of late Miocene and one sample of late Oligocene mudstone from the Barbados accretionary prism, sampled above and

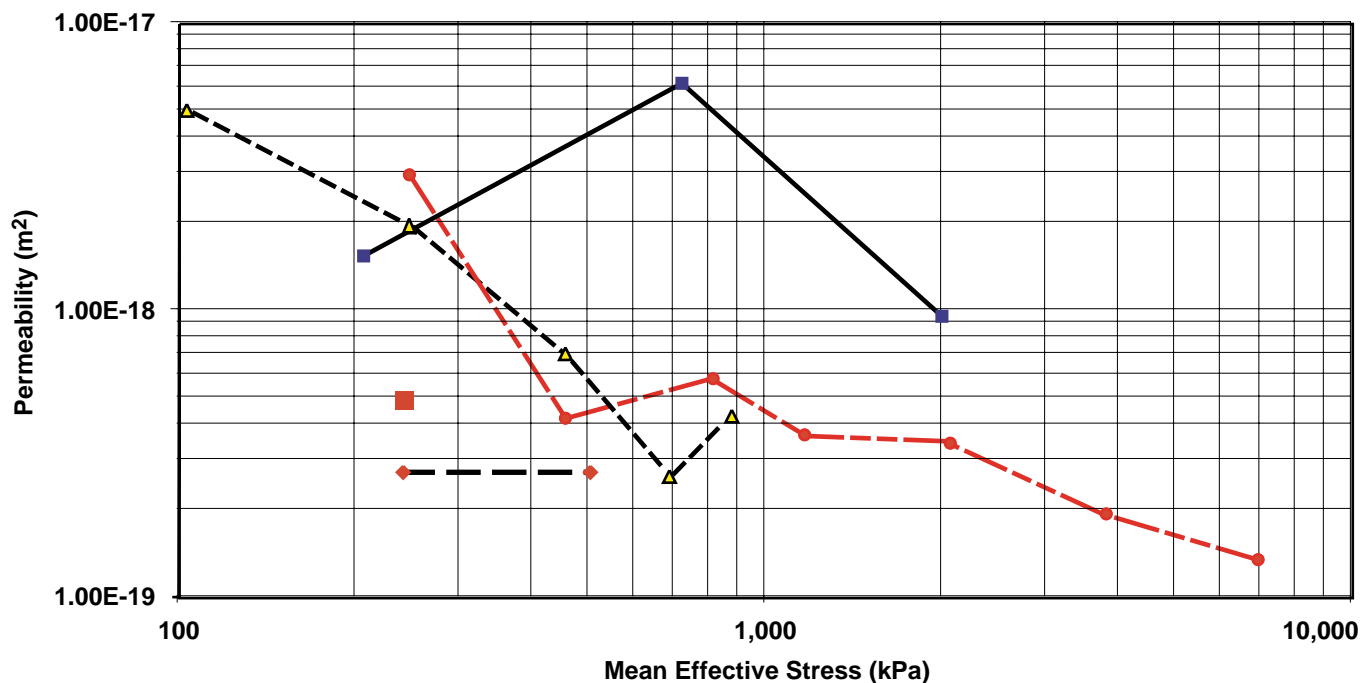


Figure 4. Permeability vs. mean effective stress. Solid line and blue = Sample 156-948C-3X-3, 89–102 cm; long dashes and red diamonds = Sample 156-948C-13X-3, 60–70 cm (Subsample a); alternating long and short dashes and red circles = Sample 156-948C-13X-3, 60–70 cm (Subsample c); short dashes and yellow triangles = Sample 156-949B-3X-2 (87–101). Isolated solid red square = permeability from constant-head test for Sample 156-948C-13X-3, 60–70 cm (Subsample b). Note how permeability generally decreases with increasing effective stress on a sample.

below the décollement zone, are similar in their mineralogical composition, consolidation history, and permeability characteristics. All of the samples are smectite rich, but less so than shipboard analyses indicate. Samples are underconsolidated by as much as 1800 kPa; this may reflect the onset of overpressure early in the samples' histories at shallow burial depths, or it may arise from a destruction of the stress history as grain contacts are perturbed by early deformation in the accretionary prism. Permeability values inferred from the consolidation response of these samples range from 10^{-18} to 10^{-19} m². In contrast to other published permeability tests, we found good correspondence between permeabilities inferred from high-stress consolidation steps and those from a single constant-head test.

ACKNOWLEDGMENTS

Andy Fisher organized shipboard collection and preservation of the core samples used in this study. Dave Webb did XRD analyses and quantitative mineralogy calculations. Ann Bishop measured grain densities and performed TGA analyses. Casey Moore and Gretchen Zwart kindly reviewed this manuscript.

REFERENCES

- Atkinson, J.H., and Bransby, P.L., 1978. *The Mechanics of Soils: An Introduction to Critical State Soil Mechanics*. London (McGraw-Hill).
- Bishop, A.W., and Henkel, D.J., 1974. *The Measurement of Soil Properties in the Triaxial Test*. London (Edward Arnold).
- Fisher, A.T., Fischer, K., Lavoie, D., Langseth, M., and Xu, J., 1994. Geotechnical and hydrogeological properties of sediments from Middle Valley, northern Juan de Fuca Ridge. In Mottl, M.J., Davis, E.E., Fisher, A.T., and Slack, J.F. (Eds.), *Proc. ODP, Sci. Results*, 139: College Station, TX (Ocean Drilling Program), 627–647.
- Fisher, A.T., and Underwood, M.B., 1995. Calibration of an X-ray diffraction method to determine relative mineral abundances in bulk powders using matrix singular value decomposition: a test from the Barbados accretionary complex. In Shipley, T.H., Ogawa, Y., Blum, P., et al., *Proc. ODP, Init. Repts.*, 156: College Station, TX (Ocean Drilling Program), 29–37.
- Moore, J.C., Shipley, T.H., Goldberg, D., Ogawa, Y., Filice, F., Fisher, A., Jurado, M.-J., Moore G.F., Rabaute, A., Yin, H., Zwart, G., and Brueckmann, W., Henry, P., Ashi, J., Blum, P., Meyer, A., Housen, B., Kastner, M., Labaume, P., Laier, T., Leitch, E.C., Maltman, A.J., Peacock, S., Steiger, T.H., Tobin, H.J., Underwood, M.B., Xu, Y., Zheng, Y., 1995. Abnormal fluid pressures and fault zone dilation in the Barbados accretionary prism: evidence from logging while drilling. *Geology*, 23:605–608.
- Moran, K., and Christian, H.A., 1990. Strength and deformation behavior of sediment from the Lesser Antilles forearc accretionary prism. In Moore, J.C., Masle, A., et al., *Proc. ODP, Sci. Results*, 110: College Station, TX (Ocean Drilling Program), 279–288.
- Moran, K., Gray, W.G.D., and Jarrett, C.A., 1995. Permeability and stress history of sediment from the Cascadia Margin. In Carson, B., Westbrook, G.K., Musgrave, R.J., and Suess, E. (Eds.), *Proc. ODP, Sci. Results*, 146 (Pt 1): College Station, TX (Ocean Drilling Program), 275–280.
- Reynolds, R.C., 1985. NEWMOD[®]—a computer program for the calculation of one-dimensional diffraction profiles of clays. Hanover, NH. (Published by the author, 8 Brook Rd.).
- Scofield, A., and Wroth, P., 1968. *Critical State Soil Mechanics*. New York (McGraw-Hill).
- Screaton, E.J., Wuthrich, D.R., and Dreiss, S.J., 1990. Permeabilities, fluid pressures, and flow rates in the Barbados Ridge Complex. *J. Geophys. Res.*, 95:8997–9007.
- Shipley, T.H., Ogawa, Y., Blum, P., et al., 1995. *Proc. ODP, Init. Repts.*, 156: College Station, TX (Ocean Drilling Program).
- Taylor, E., and Leonard, J., 1990. Sediment consolidation and permeability at the Barbados forearc. In Moore, J.C., Masle, A., et al., *Proc. ODP, Sci. Results*, 110: College Station, TX (Ocean Drilling Program), 289–308.
- Wuthrich, D.R., Screaton, E.J., and Dreiss, S.J., 1990. Fluid flow within the Barbados Ridge complex, Part II. Permeability estimates and numerical simulations of flow velocities and pore pressures. In Moore, J.C., Masle, A., et al., *Proc. ODP, Sci. Results*, 110: College Station, TX (Ocean Drilling Program), 331–341.

Ms 171AIR-108

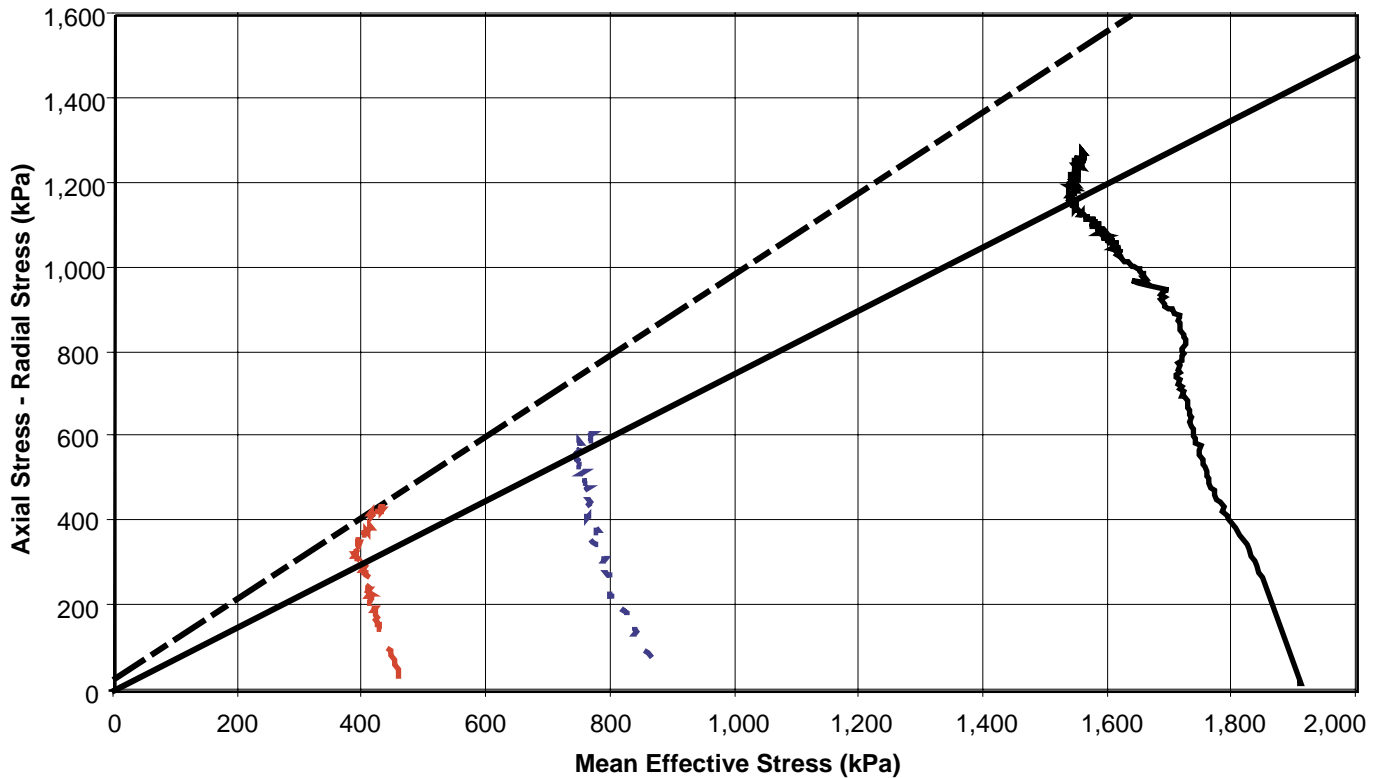


Figure 5. Stress-path plots for undrained shear strength tests. Solid black stress path = Sample 156-948C-3X-3, 89–102 cm; red dashes = Sample 156-948C-13X-3, 60–70 cm; blue dashes = Sample 156-949B-3X-2, 87–101 cm. Solid black line is the critical-state line for these samples. Note how individual stress paths—especially Sample 156-949B-3X-2, 87–101 cm—bend over and parallel this line. Sample 156-948C-13X-3, 60–70 cm, was overconsolidated during shear testing. Sample 156-949B-3X-2, 87–101 cm, may have leaked during the test, causing the stress path to become convex toward the origin. The failure envelope (alternating long and short black dashes) defined by Moran and Christian (1990) is similar to ours, but has a higher slope that may reflect a greater calcite content in the sediments tested.

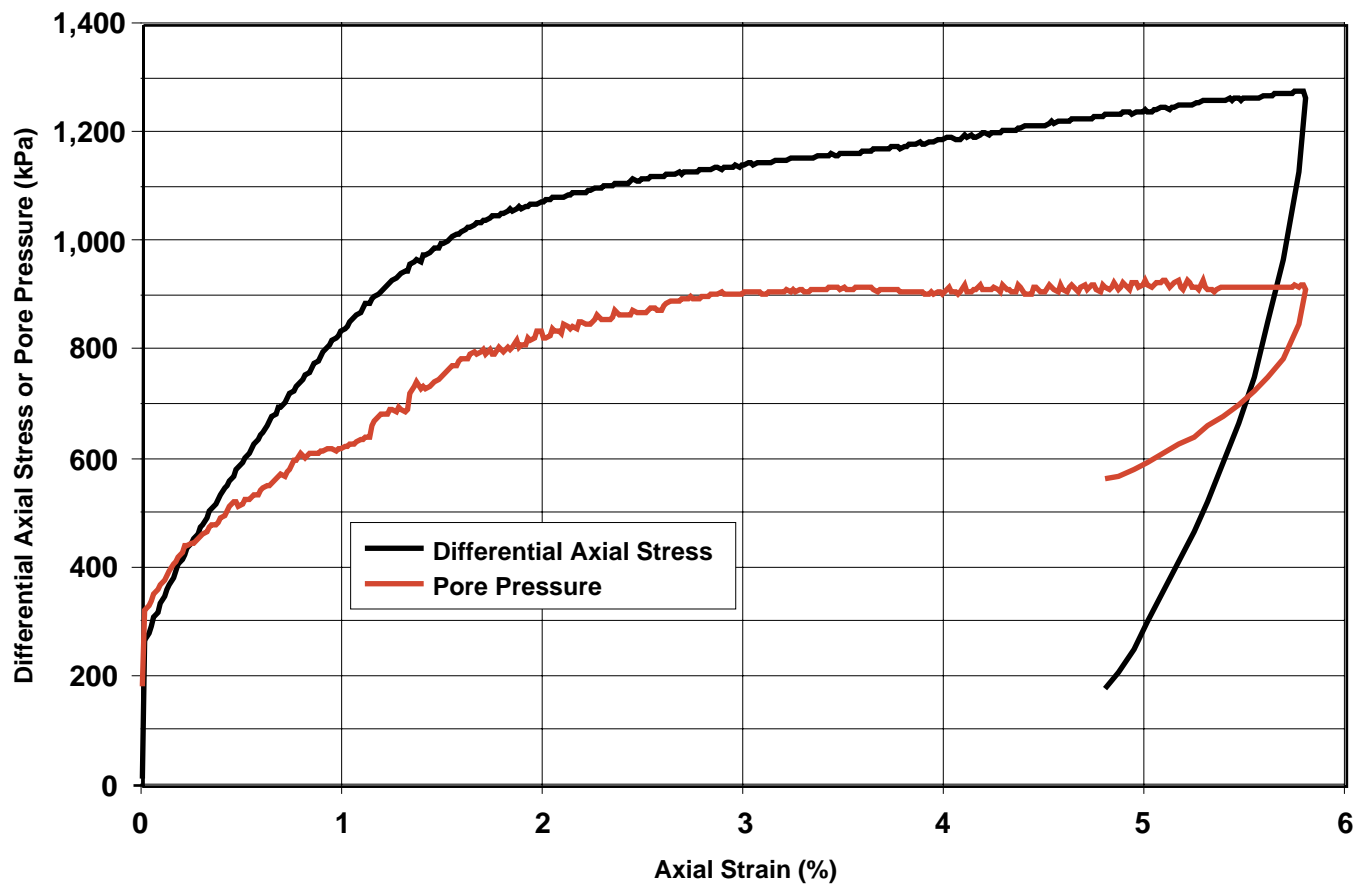


Figure 6. Stress-strain curve (Sample 156-948C-3X-3, 89–102 cm). Note that pore pressure remains constant after an axial strain of 3%–3.5% has been accumulated; the onset of constant pore pressure is interpreted as the failure point (i.e., critical-state deformation). Note the slight increase in the slope of the curve at an axial strain of 3.5%. We interpret this anomalous behavior as an experimental artifact caused by the radial strain gauge constricting the sample.